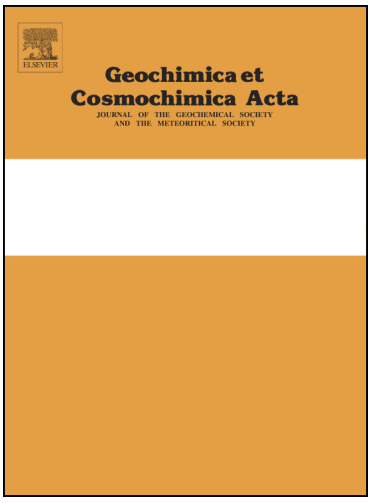

Nucleosynthetic, radiogenic and stable strontium isotopic variations in fine- and coarse-grained refractory inclusions from Allende

B.L.A. Charlier, F.L.H. Tissot, N. Dauphas, C.J.N. Wilson

PII: S0016-7037(19)30572-1
DOI: https://doi.org/10.1016/j.gca.2019.09.005
Reference: GCA 11428

To appear in: *Geochimica et Cosmochimica Acta*

Received Date: 16 September 2018
Accepted Date: 4 September 2019

Please cite this article as: Charlier, B.L.A., Tissot, F.L.H., Dauphas, N., Wilson, C.J.N., Nucleosynthetic, radiogenic and stable strontium isotopic variations in fine- and coarse-grained refractory inclusions from Allende, *Geochimica et Cosmochimica Acta* (2019), doi: https://doi.org/10.1016/j.gca.2019.09.005

Nucleosynthetic, radiogenic and stable strontium isotopic variations in fine- and coarse-grained refractory inclusions from Allende

B.L.A. Charlier[1*], F.L.H. Tissot[2], N. Dauphas[3], C.J.N. Wilson[1]

[1]School of Geography, Earth and Environmental Sciences, Victoria University of Wellington, Wellington 6140, New Zealand

[2] The Isotoparium, Division of Geological and Planetary Sciences, California Institute of Technology, Pasadena, CA 91125, USA.

[3]Origins Laboratory, Department of the Geophysical Sciences and Enrico Fermi Institute, The University of Chicago, 5734 South Ellis Avenue, Chicago, IL 60637, USA

For submission to: *Geochimica et Cosmochimica Acta*

*Corresponding author
Email address: bruce.charlier@vuw.ac.nz
Fax No: +64 (0) 463 5865
Tel. No: +64 (0) 463 5122

Abstract

We present new nucleosynthetic, radiogenic and stable Sr isotopic data from fifteen previously studied CAIs from the Allende CV3 meteorite, including the highly altered *Curious Marie* inclusion. We use double-spike TIMS techniques to determine the degrees of isotopic mass fractionation, and also present internally normalised data for the same sample digestions to permit comparisons with previous studies and couple these isotopic data with Rb, Sr, Eu and Th abundance data to consider the origins and relationships of the isotopic variations documented here. Analysed CAIs display elevated $\mu^{84}Sr$ anomalies of +58 ppm to +287 ppm, with variability far outside of analytical uncertainties (13 ppm 2 s.d.). We cannot tell at present whether these variations arise from heterogeneities in *p*-process ^{84}Sr or in the other non-radiogenic isotopes of Sr (^{86}Sr, ^{88}Sr) that are produced by the main *s*-process, weak *s*-process, and *r*-process. All inclusions fall on an offset mass-dependent fractionation line in three-isotope space ($\delta^{88/86}Sr$ vs $\delta^{84/86}Sr$) identical within error to that previously defined by bulk undifferentiated meteorites, and have a total range of $\delta^{88/86}Sr$ of ~5.3 ‰ (+1.67 ‰ to -3.67 ‰), reflecting kinetic isotope effects during partial condensation/evaporation and/or low-temperature alteration processes. CI-normalized Sr/Th ratios in our CAIs correlate with normalized Eu/Th ratios with a ~1:1 relationship, regardless of texture or Sr-isotopic values. This indicates that Sr and Eu had similar condensation behaviors with Eu condensing as Eu^{2+} and having the same chemical behavior in minerals as Sr^{2+} under conditions relevant to CAI formation in the solar nebula. Rb/Th ratios are highly variable: fine-grained CAIs display elevated Rb/Th ratios, consistent with the introduction of Rb into the CAIs by alkali-rich secondary alteration fluids. The $\mu^{84}Sr$ anomalies measured in our CAIs are similar (in magnitude) to those found in carbonaceous chondrites that formed in the outer part of the solar system. A way to reconcile this observation with the formation of CAIs near the Sun would be if the inventories of Sr and other refractory elements in carbonaceous chondrites are dominated by a cryptic refractory dust component (CRD) that was formed early and near the Sun, and was subsequently transported outwards to the carbonaceous chondrite-forming region.

1. Introduction

Among the constituents of undifferentiated meteorites, Ca, Al-rich refractory inclusions (CAIs) are unique recorders of the nebular processes that shaped the composition of planetary materials. These inclusions, most abundant in some groups of carbonaceous chondrites (MacPherson, 2014), are the oldest solids formed in the solar system (Amelin et al., 2010; Connelly et al., 2012), and are generally interpreted as representing the first solids to condense from a cooling gas of solar composition (Grossman, 1972; 1975; Beckett and Grossman, 1986; MacPherson, 2014). As such, the study of CAIs represents a unique means of constraining the processes that shaped the composition of planetary materials early in the history of the solar system. Understanding these process remains, however, challenging as the mineralogical assemblages, textures, and chemical and isotopic compositions of CAIs have been modified by processing that involved melting, evaporation, metamorphism and metasomatic alteration (Hashimoto and Grossman, 1987; MacPherson and Davis, 1993; Krot et al., 1995; Huss et al., 2006; MacPherson et al., 2012; Brearley, 2014). There is thus ongoing debate about several aspects of CAI compositions and histories.

First, there are concerns surrounding the extent to which CAIs (i) represent pristine materials condensed from the primordial solar nebula, or (ii) have been subjected to protracted and varied thermal histories (e.g. MacPherson and Davis, 1993). Coupled studies of the trace element and isotopic characteristics of CAIs can help disentangle how secondary processes have modified the primary characteristics inherited during solar nebula condensation. For example, stable isotopic analyses of Si, Mg and elemental rare-earth element (REE) abundances have proved invaluable to assess whether the compositions of CAIs are consistent with the relative volatility of elements during condensation from solar nebula gas (Lodders, 2003; Richter, 2004; Richter et al., 2007; Shahar and Young, 2007; Grossman et al., 2008a; Young et al., 2015). Similarly, many CAIs preserve distinctive, highly fractionated REE patterns that can only be explained if these elements were fractionated from one another during primary evaporation/condensation processes in the solar nebula (Boynton, 1975; Davis and Grossman, 1979). Yet, some CAIs also preserve evidence of

elemental and/or isotopic resetting (e.g. MacPherson et al., 2012) and in some cases unravelling complex histories can be difficult.

Second, there is abundant evidence that the primary mineralogies in some CAIs have been altered at some stage to form secondary minerals such as nepheline, sodalite, hedenbergite, and ilmenite (e.g. Hashimoto and Grossman, 1987; Krot et al., 2004). However, it is still unclear where this alteration took place and whether it reflects nebular and/or asteroidal process (e.g. Meeker et al., 1983; Krot at al., 1995; Russell and MacPherson, 1997). In addition to these issues around 'pristine' versus 'altered' CAIs there are unanswered questions around the controls on patterns of isotopic anomalies in bulk CAIs. The nucleosynthetic processes involved (*r*-, *s*- and *p*-process) recorded in refractory inclusions are diverse yet most CAIs show similar anomalies for a given element (the exception being the FUN inclusions, which are isotopically anomalous for many elements). An overarching explanation for this isotopic diversity is still missing, although possible interpretations have been put forward (Brennecka et al., 2013; Dauphas and Schauble, 2016). Furthermore, it is also unclear whether any stable isotope fractionation effects measured in CAIs are correlated with nucleosynthetic anomalies. Such correlations could potentially indicate the presence, then selective destruction by thermal processing of isotopically exotic pre-solar materials (Trinquier et al. 2009; Burkhardt et al., 2012; Davis et al., 2018), the FUN inclusions representing an extreme case (Papanastassiou and Wasserburg, 1978). In this regard, strontium isotopes provide a valuable perspective on the genesis and processing of CAIs.

Strontium is a refractory lithophile element with four stable isotopes: ^{84}Sr, ^{86}Sr, ^{87}Sr and ^{88}Sr, with terrestrial abundances of ca. 0.56%, 9.86%, 7.00% and 82.58%, respectively. Because the various Sr isotopes have distinct nucleosynthetic origins, Sr isotopic anomalies can trace the nucleosynthetic heritage of the solar system and provide important constraints on the genetic relationships between planets and meteorites (Dauphas and Schauble, 2016). Whereas ^{84}Sr is a *p*-process nuclide likely made in type II (core collapse; Rauscher et al., 2002) or Ia (Travaglio et al., 2004) supernovae, ^{86}Sr, ^{87}Sr and ^{88}Sr are mostly produced in two types of slow neutron capture process (*s*-process) and the rapid process of neutron capture (*r*-process).

One is the main *s*-process, which takes place in asymptotic giant branch stars (Arlandini et al., 1999; Travaglio et al., 2004; Bisterzo et al., 2014) and the other is the weak *s*-process, which takes place in massive stars. It is estimated that approximately 60% of the ^{86}Sr and ^{87}Sr is produced by the main *s*-process and the rest by the weak *s*-process (Kappeler et al., 1989; Lugaro et al., 2003). Approximately 70% of ^{88}Sr is produced by the main *s*-process and the remainder via the rapid neutron capture (*r*-process) in supernovae or neutron star mergers. A proportion of ^{87}Sr is additionally produced by the radioactive decay of ^{87}Rb ($T_{1/2}$ = 49.624 Gyr: Rotenberg et al., 2012) and the products of this decay typically dominate over possible nucleosynthetic and/or mass dependent variations in ^{87}Sr abundances. As such, the ^{87}Rb-^{87}Sr parent-daughter isotope system is a geochronological tool that has been widely used in terrestrial and meteoritic studies, and has provided important constraints on the timing of early solar system processes, most notably the timing of volatile element depletion because Rb is more volatile with respect to Sr (e.g., Papanastassiou and Wasserburg, 1969, 1978; Podosek et al., 1991; Halliday and Porcelli, 2001; Moynier et al., 2012). Finally, variations in the stable strontium isotopic ratios caused by high-temperature mass-dependent fractionation effects (Patchett, 1980a, b; Young et al., 2002; Moynier et al., 2010; Charlier et al., 2012) can also provide insights into nebular and accretionary processes.

Overall, studies of Sr isotopic variations in CAIs (and other early solar system materials) have followed three approaches.

1) Thermal Ionisation Mass Spectrometry (TIMS) or Multi-Collector Inductively Coupled Plasma Mass Spectrometry (MC-ICPMS) have been used to measure $^{87}Sr/^{86}Sr$ and/or $^{84}Sr/^{86}Sr$ ratios, with instrumental isotopic mass fractionation being corrected for by internal normalization to a fixed $^{86}Sr/^{88}Sr$ = 0.1194 (or, equivalently, $^{88}Sr/^{86}Sr$ = 8.375209). Taken at face value, high-precision data obtained in this manner indicate small but resolvable positive ^{84}Sr anomalies (expressed as $\mu^{84}Sr$ – the ppm deviation of the sample $^{84}Sr/^{86}Sr$ value from that of the NBS987 standard, now SRM987) in bulk carbonaceous chondrites (Andreasen and Sharma, 2007; Hans et al., 2013; Paton et al., 2013). However, when internal normalization is used, any information about the extent of natural stable isotopic fractionation is lost.

2) MC-ICPMS has also been used to resolve stable isotopic fractionation in one of the isotope pairs – typically $^{88}Sr/^{86}Sr$ – by using an external element to correct for instrumental mass fractionation (usually Zr) and/or employing sample-standard bracketing (e.g., Moynier et al., 2010; Charlier et al., 2012). This method, however, has a major disadvantage for cosmochemical studies in that variations in ^{84}Sr abundances cannot be accurately measured due to an isobaric interference from ^{84}Kr, which is always present to varying degrees in the Ar carrier gas used for MC-ICPMS analysis.
3) Double-spike methodologies using TIMS (Dodson, 1963; Rudge et al., 2009; Neymark et al., 2014) have been used to measure absolute Sr isotopic ratios without recourse to internal or external normalisation (Patchett 1980a, b; Charlier et al., 2017). In the pioneering early work on Allende CAIs by Patchett (1980a, b), precisions of ~0.25 ‰ and ~0.5 ‰ were obtained for the $^{88}Sr/^{86}Sr$ and $^{84}Sr/^{86}Sr$ ratios, respectively, and only broad trends in mass-dependent fractionation could be determined. The precision on the $^{84}Sr/^{86}Sr$ ratio was well below that needed to resolve any non-mass-dependent anomalies in the abundance of ^{84}Sr. With improvements in mass spectrometer technology and associated techniques, Charlier et al. (2017) identified an offset mass-dependent fractionation line in three-isotope space ($\delta^{88/86}Sr$ vs $\delta^{84/86}Sr$). Relative to terrestrial and inner solar system materials, this offset was identified at the bulk meteorite scale in several undifferentiated primitive meteorites, including Allende, indicating the survival of small, yet resolvable, nucleosynthetic anomalies in these bulk meteorites.

Here, we present new high-precision TIMS double-spike strontium isotope data and Rb/Sr relationships on dissolution aliquots from a suite of previously studied fine- and coarse-grained CAIs from Allende. We make use of Allende CAIs because of their size and abundance in the host meteorite, allowing for multiple, parallel systematics to be investigated on individual inclusions. A drawback of Allende CAIs, however, is that in contrast with CAIs from reduced examples of CV chondrites (e.g., Leoville or Efremovka), they have experienced various degrees of metasomatic alteration, presumably on the parent-body (Yurimoto et al., 2008). The suite of CAIs reported

on here has previously been investigated by Tissot et al. (2016: REE abundances and U isotopes on 15 CAIs, all of which are considered here), Tang et al. (2017: ^{26}Al-^{26}Mg and ^{36}Cl-^{36}S systematics on the unusual, U- and Mg-depleted, *Curious Marie* inclusion) and Davis et al. (2018: REE abundances and Ti isotopes on 22 CAIs, including the 15 studied by Tissot et al., 2016, and us). The work presented here is therefore part of a multi-element, multi-isotope approach that utilizes single dissolutions of single inclusions to understand the genetic relationships and processes that affected early Solar System materials, in an attempt to refine our understanding of the key formative period of our Solar System.

2. Samples and methods

2.1. Sample collection

Four coarse- and eleven fine-grained CAIs are considered in this work. Bulk sampling of the CAIs was originally carried out for the study of Tissot et al. (2016) from a number of Allende slabs. Details of the sampling techniques, and descriptions of the samples including element maps and images are in the appendix to Tissot et al. (2016). Weights of the extracted CAI samples were 16 to 473 mg (Table 1). The samples were removed from the slabs using cleaned stainless steel dental tools. Attention was paid to minimize the amount of matrix sampled with the CAI but we cannot rule out the possibility that minute amounts of matrix were present (well below 1% by volume). A fragment of each CAI was retained for imaging and *in-situ* studies, while the remainder was reduced to a fine powder and dissolved in several steps using HF/HNO_3/$HClO_4$ and HCl/HNO_3 (Tissot et al., 2016). The fragment from each CAI was mounted in epoxy and examined by backscattered electron (BSE) imaging and X-ray chemical mapping. The bulk REE characteristics of the CAIs were also measured (Tissot et al., 2016), as REE patterns of CAIs are often considered to be indicative of the evaporation/condensation processes that shaped the chemistry of those objects (Wänke et al., 1974; Davis and Grossman, 1979). The Group II REE patterns of the fine-grained CAIs are generally explained as the result of volatility controlled fractional condensation (Davis and Grossman, 1979; Kornacki and Fegley, 1986; Boynton, 1989; Tissot et al., 2016; Davis et al., 2018), whereas most coarse-grained CAIs yield REE patterns that are notably flat. One of the coarse-grained CAIs

studied here (CG-0) does display a pattern typical of Group II CAIs (i.e. volatility controlled), but over a much smaller range of elemental fractionation (e.g. the chondrite-normalised Nd/Lu ratio, a proxy for LREE/HREE fractionation, is only ~3 compared to the 20-60 range typical of Group II CAIs: Tissot et al., 2016).

The CAIs studied here range from mildly to extensively altered and consist of a variety of minerals including porous aggregates of sodalite, nepheline and grossular. As shown in the backscattered electron and element maps presented in the online materials in Tissot et al. (2016), these replace a primary assemblage of which relicts are seen as pyroxene, spinel and hibonite. The textures observed are considered to reflect extensive alteration of the primary high temperature mineralogy via the introduction of fluids rich in Ca, alkalis, H_2O, CO_2, halogens and Fe (Macpherson et al., 1988; Kimura and Ikeda, 1995). *Curious Marie* in particular is the most intensely altered of all the samples considered here and retains only vestiges of the inferred primary mineralogy (Tissot et al., 2016; Tang et al., 2017). This alteration most likely took place on the parent-body as fine-grained CAIs from reduced CV chondrites (e.g., Efremovka, Vigarano) were much less affected by aqueous alteration (Allende belongs to the oxidized CV chondrite subgroup: Yurimoto et al., 2008).

2.2. Sample processing systematics

A flow chart (Fig. S1) of the processing of the samples used for this study is given in the supplementary online materials. It details which cut was used for the Sr analyses presented here. Because the samples are elution cuts from a previous chemical separation using UTEVA resin to purify U (Tissot et al., 2016), there exists the possibility that the Sr may have become isotopically fractionated during this initial chemistry step. However, the Sr yield from the UTEVA resin is quantitative and given the high solubility of Sr in aqueous fluids, it is unlikely that Sr was fractionated during this stage. Nevertheless, to test for any fractionation, we carried out a series of tests using the US Geological Survey geostandard BHVO-2, where we compared the same standard unprocessed and processed through UTEVA columns and analyzed in the same fashion as the unknowns. No effect of the UTEVA resin could be discerned on Sr yields, or Sr isotopic characteristics (see supplementary online materials). Sr blanks were in the tens of pg range and were considered negligible

against the >>100 ng Sr load amount measured for both the natural and double-spiked Sr sample aliquots. As a result, no blank corrections were made to the Sr isotopic data.

2.3. Mass spectrometry

The $^{87}Rb/^{86}Sr$ ratios were measured on a Thermo-Fisher Element 2 sector field ICP-MS at Victoria University of Wellington (VUW). Sr-isotopic mass spectrometry measurements were carried out using a Thermo-Fisher Triton TIMS instrument, also at VUW. Details of the analytical protocols, including double spiking, chemical separation and TIMS analysis are given in Charlier et al. (2017) and summarised in the supplementary material. The TIMS measurements were carried out within a single analytical session over an approximately two-week period. This approach provided an internally consistent, high-precision dataset and circumvented any issue of longer-term fluctuations in the measured isotope ratios that might have arisen from Faraday cup degradation. Estimates of precision and blanks pertaining to this study are given in the online supplementary material (Table S1).

3. Results

For the purposes of this paper we first present separately the different facets of Sr isotopic variations in CAIs, focusing on (1) nucleosynthetic anomalies using internally normalized data to allow comparisons with earlier work, (2) radiogenic ingrowth from ^{87}Rb coupled with consideration of the Rb, Sr elemental concentrations, and (3) stable isotopic variations utilizing double-spike data. The data are summarised in Table 1.

3.1. Internally normalised $\mu^{84}Sr$ data

Strontium has only four stable isotopes, with ^{87}Sr including a radiogenic component from the decay of ^{87}Rb. This means that after internal normalization to $^{86}Sr/^{88}Sr$ = 0.1194 (or, in exact equivalence, $^{88}Sr/^{86}Sr$ = 8.375209: Rosman & Taylor, 1997), only the $^{84}Sr/^{86}Sr$ ratio can be used to discuss isotopic anomalies. We use internally normalized data at this point to allow direct comparisons with the earlier published data. We revisit the ^{84}Sr anomalies later (section 4) in the context of the mass-

dependent data derived from the double-spike analyses. The internally normalized $^{84}Sr/^{86}Sr$ ratios of the samples are reported here in $\mu^{84}Sr$ notation, which represents the parts per 10^6 deviation from the average $^{84}Sr/^{86}Sr$ ratio for the NBS987 Sr isotope standard determined for the period of analysis of this study. The data are shown in Fig. 1, along with $\mu^{84}Sr$ data from published studies of Allende CAIs. The external reproducibility of our $\mu^{84}Sr$ standard values of 14 ppm (2 s.d.) is significantly smaller than that obtained in several of the previous studies. Our CAI data span the same range of $\mu^{84}Sr$ values previously reported including a sample that returns an unusually high $\mu^{84}Sr$ value approaching +300. A mean $\mu^{84}Sr$ value of all the CAI data plotted in Fig. 1 is +124 ± 98 (2 s.d., ± 13, 2 s.e., *n* = 53), coincident with the peak in the relative probability curve at a $\mu^{84}Sr$ value of ~+125. The mean of our data set alone is +110 ± 122 (2 s.d., ± 32, 2 s.e., *n* = 15). Fine-and coarse-grained CAIs have similar $\mu^{84}Sr$ anomalies, defining average values of +106 ± 140 (2 s.d., ± 42, 2 s.e., *n* = 11), and +123 ± 57 (2 s.d., ± 29, 2 s.e., *n* = 4), respectively. As is apparent from Fig. 1 and the high calculated standard deviations of the average values for these populations, there is considerable heterogeneity in $\mu^{84}Sr$ values that well exceeds analytical uncertainties. Because of this large variability we do not present these data as simple weighted means as many of the values are resolvably distinct at the quoted level of precision. Myojo et al. (2018) also found variations well outside of analytical precision for $\mu^{84}Sr$ within a single CAI, implying the existence of additional heterogeneity below the scale of whole CAI sampling.

3.2. Internally normalized $^{87}Sr/^{86}Sr$ and $^{87}Rb/^{86}Sr$ data

In Fig. 2, we plot $^{87}Sr/^{86}Sr$ ratios (internally normalized using the exponential law to $^{88}Sr/^{86}Sr = 8.375209$ following convention: Rosman and Taylor, 1998) versus $^{87}Rb/^{86}Sr$ in an isochron diagram. On this figure, the least radiogenic points are the coarse-grained CAIs whilst the fine-grained CAIs all have significant amounts of radiogenic ingrowth in $^{87}Sr/^{86}Sr$ coupled with much higher $^{87}Rb/^{86}Sr$ ratios due to the addition of Rb (and other alkalis) in fine-grained CAIs by an early alteration event, the location and setting of which is uncertain but could have been the parent-body of Allende.

Using the model 3 fit of Isoplot (which assumes that the scatter is due to a combination of assigned errors plus a normally distributed variation in the Y-values; Ludwig, 2002) and an ^{87}Rb decay constant of 1.3971×10^{-11} yr^{-1} (Rotenberg et al., 2012), the data scatter about a best-fit line that yields a model age of 4507 ± 23 Ma and an initial $^{87}Sr/^{86}Sr = 0.69886 \pm 19$ (MSWD = 69, *n* = 15) for all the CAIs analysed. This model age is inconsistent with existing U-Pb-derived estimates for the primary formation ages of CAIs of ~4567-4568 Ma (e.g. Amelin et al., 2010; Connelly et al., 2012). The high MSWD for the errorchron reflects a considerable degree of scatter in the data for the fine-grained CAIs, accompanying a wide range in $^{87}Rb/^{86}Sr$ ratios, from 0.0041 to 1.469. The most extreme example is the grain *Curious Marie* that has an unusually high $^{87}Rb/^{86}Sr$ ratio (1.469) and consequently high measured $^{87}Sr/^{86}Sr$ ratio (0.794450). The coarse-grained CAIs in contrast have a restricted range in $^{87}Rb/^{86}Sr$ ratios (0.0041 to 0.056) and have measured $^{87}Sr/^{86}Sr$ values ranging from 0.699198 to 0.702554.

3.3. Double-spike stable Sr data

In Fig. 3, the data (Table 3) are plotted in three-isotope space ($\delta^{88/86}Sr$ vs. $\delta^{84/86}Sr$) using the δ permil units referenced to NBS987 (see supplementary material). A key point about our new CAI data is that they extend to both high and low $\delta^{88/86}Sr$ values relative to the bulk Earth value of ~0.29 ‰ as defined by Moynier et al. (2010) and Charlier et al. (2012). The data form a correlation line on the three-isotope plot and cover a total range of ~5.3 ‰ in $\delta^{88/86}Sr$, from +1.67 to -3.67 ‰. A linear regression (Model 3 implemented in Isoplot: Ludwig, 2002) yields a line with slope -0.988 ± 0.023 (2 s.d.; MSWD = 25) which passes through an *x*-intercept value of $\delta^{84/86}Sr = 0.144 \pm 0.037$ ‰. In comparison, a line defined by samples of bulk, primitive meteorites (Charlier et al., 2017) has an identical slope within error of -1.00 ± 0.21 (MSWD = 7.5) and has a similar (within error) *x*-intercept at $\delta^{84/86}Sr = 0.094 \pm 0.028$ ‰. The slope value of the best fit line presented here corresponds to the theoretical expectation for mass-dependent fractionation which stipulates that the relative isotopic variations scale as the difference in the absolute masses of the isotopes involved; $(^{84}Sr\text{-}^{86}Sr)/(^{88}Sr\text{-}^{86}Sr) \sim -1.0$. Because the degree of stable isotopic variations along the mass-dependent fractionation line (MDFL) is much larger than the isotopic anomalies displaced from the MDFL, the two can be discussed

independently and in the following, we use $\delta^{88/86}Sr$ to denote the degree of mass-dependent isotopic fractionation.

For comparative purposes we also show seven feldspar analyses from angrite meteorites (from Charlier et al., 2017). Angrites, a group of ancient achondrites, are the most volatile-element depleted among all meteorite groups, and are inferred to represent a planetary body (Keil, 2012) that is among the earliest known differentiated inner Solar System material (Tissot et al., 2017 and references therein). These data fall on a different correlation line than those defined by the bulk primitive meteorite (Charlier et al., 2017) and CAI data. The former line has an intercept ($\delta^{88/86}Sr$ = -0.001 ± 0.029 ‰) that is indistinguishable within error from the terrestrial composition. The angrite feldspar data are part of a larger suite of terrestrial, lunar and differentiated meteorite samples that appear to have been derived from a reservoir devoid of Sr isotopic anomalies relative to Earth (Charlier et al., 2017). The slopes calculated for (a) the best fit line for the CAIs and bulk primitive meteorites together, and (b) the line for the angrite data (Charlier et al., 2017), are identical within errors to those calculated for equilibrium or kinetic mass-dependent fractionations (Young et al., 2002; Dauphas and Schauble, 2016).

4. Discussion

To assess what processes controlled the chemistry and Sr isotopic compositions of CAIs, the above data are now coupled with the REE and other trace element data from Tissot et al. (2016).

4.1. Nucleosynthetic anomalies ($\mu^{84}Sr$)

As explained earlier, for the purposes of comparing our $\mu^{84}Sr$ values with published data we calculated the difference between each of the internally normalized $^{84}Sr/^{86}Sr$ values of the samples and those of the average value for the NBS987 standard (see Supporting Online Materials). In this regard, the use of a fixed $^{86}Sr/^{88}Sr$ ratio for the internal normalization conceals the possibility that the anomalies lie in isotopes other than ^{84}Sr, but the data (as in all studies in the Sr isotopic system, with its four isotopes) do not allow this to be unambiguously

resolved. Here, the data are corrected for mass fractionation using the exponential law. As presented in Section 3.3, the CAIs record significant mass-dependent fractionation. If the natural mass-fractionation experienced by the CAIs does not follow the exponential law, this could produce spurious isotopic anomalies after normalization of the mass spectrometric data to the exponential law in cases where the $^{88}Sr/^{86}Sr$ fractionation is large (see next paragraph). This effect has been discussed elsewhere extensively in the literature in the context of $\delta^{26}Mg$ and an early solar system chronology from ^{26}Al-^{26}Mg systematics (Jacobsen et al., 2008; Wasserburg et al., 2012; Davis et al., 2015; Boehnke et al., 2018), and for Ni isotopic anomalies (Tang and Dauphas, 2012).

In the context of the Sr data presented here, the generalized power law, a formalism describing mass fractionation through a single free parameter, *n* (Maréchal et al., 1999), was used to assess the impact of different mass fractionation laws where *n* = -1 (equilibrium law; EqLaw), $n \longrightarrow 0$ ($n = 10^{-6}$; exponential law; ExpLaw) and *n* = 1 (power law; PLaw). These parameters were used to derive β-values (slope of the mass fractionation line, here in $\ln^{84}Sr/^{86}Sr$ vs. $\ln^{88}Sr/^{86}Sr$ space, where $\beta_{EqLaw} = -1.0473$, $\beta_{ExpLaw} = -1.0232$ and $\beta_{PLaw} = -0.9997$). The slopes of the predicted fractionation correlation lines in ln-Sr isotope space were then used to calculate the deviations in $\mu^{84}Sr$ with reference to the exponential law. As shown in Fig. 4, the total range in $\delta^{88/86}Sr$ is ~5.32 ‰. Over this range, all CAIs are resolvably offset from $\mu^{84}Sr = 0$, regardless of their degrees of mass-dependent fractionation. Furthermore, there is no evidence of a correlation between $\delta^{88/86}Sr$ and $\mu^{84}Sr$. The correction for natural mass-fractionation using the exponential law can induce a bias across the full range in $\delta^{88/86}Sr$ values of at most ~12.5 μ-units (that is, the total range in $\mu^{84}Sr$ values between the different fractionation laws across the entire range of $\delta^{88/86}Sr$ values measured in this study: Fig. 4). Therefore, selection of an inappropriate fractionation correction cannot be a significant factor in influencing the inter-CAI variability in $\mu^{84}Sr$ values documented here.

The CAI $\mu^{84}Sr$ values we obtain cover a range similar to those reported by the earlier authors cited in Fig. 1. However, the high precision of our data allows us to resolve significant dispersion in the $\mu^{84}Sr$ values (particularly for fine-grained CAIs),

reflected in the large 2 s.d. value, in agreement with the recent data from Myojo et al. (2018). Earlier studies (Fig. 1) yielded more uniform values (albeit with lower precision) and it is not clear from the mineralogical data available whether the differences result from the samples being from contrasting CAI types or reflect analytical differences. Our data and those of Myojo et al. (2018) imply the presence of heterogeneity between inclusions. In addition, variations recorded by Myojo et al. (2018) from a single FTA inclusion demonstrated an intra-grain $\mu^{84}Sr$ heterogeneity beyond analytical uncertainties. Overall, their data and ours point to the existence of an ^{84}Sr-enriched component that is present in some inclusions. One possibility is that this represents a nugget effect if the number of carrier grains of ^{84}Sr anomalies in each CAI is sufficiently low that Poisson statistics will produce a heterogeneity in $\mu^{84}Sr$ of the magnitude detected here. This effect cannot be fully quantified at this stage because the mass abundances, Sr concentrations and isotopic leverage of any putative ^{84}Sr-enriched nuggets are all undetermined. However, when the $\mu^{84}Sr$ values of the CAIs are plotted versus the sample mass dissolved (Fig. 5), we find more scatter in $\mu^{84}Sr$ values for smaller sample masses, which would be qualitatively consistent with the presence of more- or less- positive $\mu^{84}Sr$-bearing nuggets. Our data demonstrate that if a nugget effect is present, it is influencing the bulk CAI samples towards positive $\mu^{84}Sr$ values. Paton et al. (2013), in their leachate study of CI chondrite Ivuna found large negative $\mu^{84}Sr$ anomalies, suggesting that several presolar carriers may have influenced isotopic anomalies of meteorites and their components.

4.2. Rb/Sr systematics

A first-order distinction in our data is between the coarse-grained CAIs, which have low Rb abundances, low $^{87}Rb/^{86}Sr$ ratios and consistently very primitive $^{87}Sr/^{86}Sr$ ratios, and the fine-grained inclusions which have elevated Rb abundances and $^{87}Rb/^{86}Sr$ ratios, and correspondingly large amounts of radiogenic Sr ingrowth (Fig. 2). As shown in the ^{87}Rb-^{86}Sr evolution diagram, all the CAI data fall along a 4.507 ± 0.023 Ga correlation line with an initial $^{87}Sr/^{86}Sr$ ratio of 0.69886 ± 20. Because of the relatively large uncertainty associated with the fit of this line, we can only say that our initial value for all the CAIs analysed agrees (within error) with the ranges

in initial CAI $^{87}Sr/^{86}Sr$ values proposed for the 'ALL' CAI 'D7' = 'USNM#3898' by Gray et al. (1973: 0.69877 ± 4), and other CAIs by Podosek et al. (1991: 0.698916 ± 20), Hans et al. (2013: 0.698935 ± 9), and Nyquist et al. (2004: 0.698934 ± 15). Note that the first value is as reported, with no standard normalisation (see Hans et al., 2013; Papanastassiou, 2015), while the later three values are reported with standard normalisation to NBS987 $^{87}Sr/^{86}Sr = 0.710250$. The apparent timing implied by the correlation line is more recent than the chronologies for alteration yielded by Mn-Cr (3.7 ± 0.7 Myr after CAI formation: MacPherson et al., 2015) and ^{129}I-^{129}Xe systematics (3.8-4.5 ± 0.3 Myr after CAI formation: Pravdivtseva et al., 2003) in CV3 meteorites, including Allende. It is, however, resolvably older than an ^{87}Rb-^{86}Sr internal isochron of 4247 ± 110 Myr from mineral fractions from an Allende CAI reported by Marks et al. (2014). The observed scatter in the full data set about the best fit line (MSWD = 69), contributing to the large uncertainty on the calculated errorchron age and $^{87}Sr/^{86}Sr_i$ intercept, is indicative of open system processes (e.g. decoupling of Rb from Sr during alteration), such as the later addition of Rb during impact events. Any accidental, physical admixture of matrix during sampling of the CAIs may be reflected in this scatter, but large-scale incorporation of matrix is precluded by the trace-element data discussed in the next paragraph.

To examine open system behavior, we consider the variability in the ratio of Rb and Sr abundances relative to those of an immobile element (Th in this sample set, from Tissot et al., 2016), normalised to CI chondrite values (Fig. 6a). The fine-grained CAIs show an increase in Rb/Th correlated with Sr/Th. On the other hand, in all coarse-grained inclusions, Rb/Th ratios remain distinctly lower while the Sr/Th ratios increase. These data imply that the distributions of Rb and Sr between fine-and coarse-grained CAIs are decoupled, as also reflected in the poor fit and high MSWD of the errorchron in Fig. 2. Such decoupling may explain why the 4507 Ma age of the errorchron is younger than other estimates of the timing of alteration for CAIs. The variations in the Sr/Th ratio in fine-grained CAIs are largely controlled by variations in the concentration of the fluid-immobile Th.Sr varies by a factor of ~3 among fine-grained CAIs while Th varies by a factor of ~8: the Sr/Th ratio thus primarily correlates with the Th concentration. The reason why the Sr/Th ratio correlates broadly with the Rb/Th ratio among fine-grained CAIs might thus be that Rb was

introduced by aqueous alteration in a constant amount in the porous fine-grained CAIs, and both the Rb/Th and Sr/Th ratios are driven by variations in the concentration of Th. Note that these variations cannot simply reflect incorporation of matrix material during sampling as Na abundances vary between 0.2 and 23 x CI and Ca between 2.8 and 21x CI (Tissot et al., 2016), consistent with the extreme care that was taken to minimize matrix contamination during sample extraction, and the less than ~1% by mass contamination estimated based on visual inspection. Even the coarse-grained CAIs that are most closely representative of complete condensation of refractory elements (on the basis of their flat REE profiles: Davis et al., 2018) still have detectable Rb contents that have influenced their present-day radiogenic Sr-isotopic characteristics (Fig. 2).

It is unlikely that variations in the Sr/Th ratio solely reflect introduction of Sr by aqueous alteration because the normalised Sr/Th values correlate with normalized Eu/Th ratios along a 1:1 correlation line (Fig. 6b). Variations in Eu abundances in CAIs, in particular fine-grained examples, have been previously ascribed to incomplete condensation of Eu, which is one of the most volatile REE (together with Yb: Boynton, 1989; Davis et al., 2018). Models for the condensation of solar nebula gas predicts that Eu should have behaved differently to Sr and been incorporated into contrasting mineral phases (Grossman et al., 1977; Lodders, 2003). However, contrary to any theoretical expectations, our data (Fig. 6b) show that Sr and Eu are strongly coupled.

4.3. Stable isotopic fractionation

The stable strontium isotopic compositions of the CAIs are shown on a three-isotope plot (Fig. 3) which informs on stable isotopic fractionation processes (condensation/evaporation/mixing) operating during the formation of these CAIs. When compared with the bulk undifferentiated meteorite data from Charlier et al. (2017) (ranging from +0.32 to -0.09 ‰), and the average terrestrial $\delta^{88/86}$Sr value (+~0.29 ‰; Moynier et al., 2012; Charlier et al., 2012) the CAI data extend to both heavier and lighter values for $\delta^{88/86}$Sr (ranging from 1.69 to -3.64 ‰). When Sr abundances are ratioed to a refractory element such as Sm (Fig. 7), theoretical considerations for different pathways of evaporation/condensation/mixing can be

explored to study the variations in $\delta^{88/86}$Sr, if it is assumed that all the isotopic variations are inherited from high-temperature processes. The Sr isotopic compositions in our fine-grained CAI samples are asymmetrically distributed towards light $\delta^{88/86}$Sr values (Figs. 3 and 7). Such light enrichments could be explained by kinetic effects during condensation (Richter, 2004; Dauphas and Rouxel, 2006; Simon and DePaolo, 2010; Dauphas et al., 2015). This is because the kinetic theory of gases predicts that light isotopes tend to impinge on surfaces at a higher rate than heavy isotopes. To first order, the fractionation can be as large as the square root of the masses of the isotopes involved, i.e., -11.4 ‰ for the ^{88}Sr/^{86}Sr ratio, but will be lower if the gas is not supersaturated (Richter, 2004, Dauphas and Rouxel, 2006; Simon and DePaolo, 2010; Dauphas et al., 2015). With no supersaturation, the vapor would be in thermodynamic equilibrium with the condensate and no kinetic isotopic fractionation would occur. The values observed in the fine-grained CAIs reach ~-3.6 ‰ $\delta^{88/86}$Sr. The gas left behind from condensation of such material would be enriched in the heavy isotopes of Sr and further condensation from such gas could explain the average heavier Sr isotope composition measured in fine-grained samples. Equilibrium fractionation at the high temperatures involved in CAI formation is undoubtedly much lower than the total range in $\delta^{88/86}$Sr of 5.33 ‰ measured here. We thus conclude that the stable isotopic compositions of Sr in the (type II) CAIs analyzed here primarily reflect kinetic isotope effects associated with condensation along with the possibilities of both partial evaporation and/or recondensation (cf. Niederer and Papanastassiou, 1984; Simon et al., 2017). Similar inferences were reached with Ti stable isotope variations on these (Davis et al., 2018), and other samples (Simon et al., 2017). The CAIs investigated by us and Davis et al. (2018) display both heavy and light Ti isotopic compositions and there is a tendency for the CAIs with more fractionated REE patterns (i.e., fine-grained) to display more variable Ti isotopic compositions. Mass-dependent fractionation effects in Ca isotopes were also documented in other Allende CAIs (Niederer and Papanastassiou, 1984) and attributed to multiple stages of condensation, evaporation and re-condensation in the solar nebula.

A complementary perspective can be derived from plotting the elemental Rb concentrations, $\delta^{88/86}$Sr and μ^{84}Sr values against Sr concentrations. Increasing Sr

(and Rb) values in our fine-grained inclusions and those of Patchett et al., 1980a (Fig. 8a) accompany a decrease in the range of $\delta^{88/86}$Sr values (Fig. 8b), but are not reflected in any systematic μ^{84}Sr variations (Fig. 8c). For our coarse-grained inclusions there is a general clustering – regardless of the Sr abundances – at a $\delta^{88/86}$Sr value of ~-0.5 (i.e., approximately the mid-point of the range in $\delta^{88/86}$Sr values: see Fig. 3). The samples that are most depleted in Sr show that largest scatter in $\delta^{88/86}$Sr, suggesting that they have been most thermally processed. We note, however, that the distribution in $\delta^{88/86}$Sr values is always centered around the same value of ~-0.5, regardless of the degree of depletion in Sr. The reason for that is unclear but it could be that both evaporation and condensation were at play simultaneously, so that both light and heavy Sr isotope enrichments were manifested. If, for sake of argument, it is inferred that all the Rb in our samples has been introduced by metasomatic alteration fluids, then two points are apparent. First, in the fine grained inclusions studied by us and Patchett (1980) there is a quasi-systematic relationship with elemental Sr abundances, accompanying a wide range in $\delta^{88/86}$Sr and $\delta^{84/86}$Sr values. This would imply that the alteration processes have influenced the stable and nucleosynthetic isotopic ratios (Fig. 3) through mass-dependent fractionation while at the same time the Sr and Eu remain coupled (Fig 6b). Second, the coarse-grained inclusions have minor amounts of Rb (<7 ppm) despite Sr varying from 100 to 240 ppm, coupled with a narrow range of $\delta^{88/86}$Sr values (Fig. 3) and retaining the close linkage between Sr and Eu (Fig.6). This would imply that if the Rb is a secondary introduction, then so also is the Sr to a greater or lesser extent. However, this does not accompany any change in the nucleosynthetic μ^{84}Sr patterns.

Note also that the overall offset MDFL in $\delta^{84/86}$Sr versus $\delta^{88/86}$Sr space measured from the CAI suite analyzed here matches that previously observed by Charlier et al. (2017) in data from undifferentiated bulk meteorites (including Allende). We therefore infer that the overall $\delta^{88/86}$Sr variations represented in the inclusions studied here reflect dominantly mass-dependent fractionation processes operating on material that shares Sr-isotopic characteristics in common with the outer solar system domain, on account of their distribution along the 'offset' MDFL (Fig. 3) as

discussed in Charlier et al. (2017). We return to the contrasting isotopic evidence for the origin of the CAIs in section 4.6.

4.4. Ambiguity of *p*- versus *r*/*s*-process anomalies in bulk CAIs

The $\mu^{84}Sr$ values shown in Fig. 1 can be most simply considered to represent an excess in *p*-process ^{84}Sr. The alternative, namely that there are variations in *r*-process ^{88}Sr that influence the conventional $^{86}Sr/^{88}Sr$ ratio (0.1194) used for internal normalization, cannot be uniquely addressed here. What is required to discriminate between these alternatives is to either (1) find the carrier of the nucleosynthetic anomalies, or (2) measure samples with extremely low $^{87}Rb/^{86}Sr$ ratios, for example, CAIs from reduced CV3 samples. In the latter case, such samples would record close to the initial $^{87}Sr/^{86}Sr$ ratio (and require minimal age correction) to test the conformity of the double spike-derived $^{87}Sr/^{86}Sr$ data to a mass-dependent fractionation line in $^{87}Sr/^{86}Sr$- $\delta^{88/86}Sr$ space.

In this study, we attempt to use our coarse-grained, Rb-poor CAI data to address these issues. In Fig. 9, we plot the age-corrected (to 4507 Ma, derived from Fig. 2), double-spike $^{87}Sr/^{86}Sr$ values for our CAI data, then highlight (in panels b and c) data for the four coarse-grained samples versus the relevant double-spike derived $\delta^{88/86}Sr$ and $\delta^{84/86}Sr$ values. This approach eliminates the minor radiogenic contribution and allows the effects of mass-dependent fractionation to be compared against what Neymark et al. (2014) term the "…"true" $^{87}Sr/^{86}Sr_N$ values…". Data from the four CAIs fall on a line in panel b ($\delta^{88/86}Sr$)with a slope of 0. 0003511 ± 43 (MSWD = 3.9) and in panel c ($\delta^{84/86}Sr$) with a slope of -0.0003703 ± 17 (MSWD = 0.22) These values can be compared to those of theoretical equilibrium MDFLs calculated from the isotopic mass ratios (0.000353 for $\delta^{88/86}Sr$ and -0.0003488 for $\delta^{84/86}Sr$) , using the methods of Young et al. (2002). In contrast, application of this approach to the fine-grained CAIs is precluded by the large age correction required to these points with large $^{87}Rb/^{86}Sr$ values, such that a line drawn through the fine-grained CAI data set alone has a slope of 0.00045 ± 11 with a MSWD of 8627, indicating that the initial $^{87}Sr/^{86}Sr$ ratio cannot be reliably determined on our data, or shown to conform to a mass-dependent fractionation line.

Our internally normalised $^{87}Sr/^{86}Sr$ data for coarse-grained CAIs alone yield an initial value (0.698914 ± 17: Fig. 2) which is coincident within error of those reported by Podosek et al. (1991), Nyquist et al. (2004) and Hans et al. (2013). However, Hans et al. (2013) argued that the apparent offset to positive $\mu^{84}Sr$ values (Fig. 3 here) reflected anomalies in the $^{88}Sr/^{86}Sr$ ratio used for normalization. On that basis they adjusted their $^{87}Sr/^{86}Sr$ initial estimate upwards to 0.698975 ± 8 to account for this anomaly, resulting in a corrected value closely matching the classic basaltic achondrite best initial (BABI) value of $^{87}Sr/^{86}Sr$ = 0.69899 (Papanastassiou and Wasserburg, 1969). If the offset between the two MDFLs shown in Fig. 3 (and identified by Charlier et al., 2017) is real, it cannot be uniquely decided whether the offset is vertical (due to *r*-process ^{88}Sr variations, or variable contributions of the main and weak *s*-processes) or horizontal (due to *p*-process ^{84}Sr variations), or some combination of the two. In turn, on this basis, we cannot uniquely demonstrate whether the difference in reported initial $^{87}Sr/^{86}Sr$ ratios between primitive, undifferentiated meteorites (e.g. that derived from the value of the CAI "D7" = "USNM#3898": Gray et al., 1973; MacPherson et al., 2018) and differentiated planetary material (e.g. BABI and the angrite initial $^{87}Sr/^{86}Sr$, ADOR: Hans et al., 2013) is rea,l or an artefact of normalization to a value that is no longer canonical due to variability in *r*-, main *s*- or weak *s*-process proportions. We would, however, point out that studies of the Sr isotopic variations in FUN inclusions have reported no significant anomalies in initial $^{87}Sr/^{86}Sr$ ratios for refractory inclusions where $\mu^{84}Sr$ values are offset by hundreds to thousands of ppm (Papanastassiou and Wasserburg, 1978; Amelin et al., 2015; Papanastassiou, 2015; Papanastassiou and Chen, 2016). These observations imply that the canonical $^{88}Sr/^{86}Sr$ ratio used for normalization is close to the real value and that the anomalies most probably lie in ^{84}Sr, reflecting a *p*-process variability, if FUN and normal CAIs are considered to share similar Sr-isotopic characteristics relative to terrestrial and differentiated objects.

In considering this issue of ^{84}Sr heterogeneity, note that Paton et al. (2013) found positive $\mu^{84}Sr$ values for early leach steps of the Ivuna type-CI chondrite (and for their reconstituted "bulk" data) that closely match our values, but strongly negative $\mu^{84}Sr$ values for the trace amounts of Sr represented in two chemically resistant

aliquots. The latter values were taken to indicate an *r*-process deficit in ^{88}Sr that resulted in an apparently lower $^{84}Sr/^{86}Sr$ ratio after normalisation to $^{86}Sr/^{88}Sr$ = 0.1194. Similarly, Yokoyama et al. (2015) reported negative $\mu^{84}Sr$ values for refractory leach steps in the Murchison and Tagish Lake chondrites. However, all their leach-step $\mu^{84}Sr$ values from three bulk Allende samples remained positive and between 39 and 119 ppm. These results (and the FUN data) clearly indicate that there is a diversity in relative proportions of ^{84}Sr that are as yet unresolved.

4.5. Fine-grained vs. coarse-grained CAIs

Although the consensus is that CAIs formed in a region close to the proto-sun (e.g. Scott and Krot, 2014; MacPherson, 2019), on the basis of their distinctive Sr-isotopic compositions on the 3-isotope plot (Fig. 3; cf. Charlier et al., 2017) the fine- and coarse-grained CAIs both show isotopic affinities with carbonaceous chondrites that most likely formed far from the Sun (Fig. 10). However, recent studies of the nucleosynthetic anomalies in Mo isotopes preclude a simple genetic relationship between these two classes of inclusions (Brennecka et al., 2017; Tissot et al., 2019), because fine-grained CAIs show variations in *s*-process Mo, whilst coarse-grained CAIs show a near constant excess in *r*-process material. This difference in Mo isotopic anomalies implies that the two main types of CAI formed in two mostly separate source reservoirs, separated either spatially and/or temporally. In contrast, for Sr (as shown here) and many other isotopic systems (e.g. Cr, Ti, Ba, Nd, Sm, Er, Yb, Hf: Dauphas and Schauble, 2016 and references therein; Brennecka et al., 2017; Davis et al., 2018; Scott et al., 2018; Shollenberger et al., 2018a, b), fine-grained and coarse-grained CAIs share largely overlapping isotopic anomalies. The reason why fine- and coarse-grained CAIs show similar anomalies in some elements but distinctive anomalies in others is uncertain but it could be due to different thermal processing of their precursor materials that could have partially destroyed/homogenized specific pre-solar grain carriers. Such a difference in thermal processing is seen in the more prevalent presence of group II REE patterns in fine-grained CAIs compared to coarse-grained CAIs (where this pattern is extremely rare), and the larger dispersion in Sr and Ti isotopic compositions in fine-grained CAIs compared to their coarse-grained counterparts (Tissot et al., 2016; Davis et al., 2018).

4.6. A CAI conundrum?

The Sr-isotopic data we present here for CAIs from Allende, when coupled with the complex array of isotopic data from other elements in CAIs and the array of solar system materials, highlights and adds further to a conundrum in the origin and evolutionary history of CAIs (e.g. Desch et al., 2018). Numerous lines of evidence point towards the origin of CAIs in high-temperature regions close to the sun, almost certainly closer than the orbit of Jupiter (e.g. Scott et al., 2018; MacPherson, 2019). These include the following. (1) CAIs are ^{16}O-enriched relative to chondrules, and fall close to the solar value along a mass-dependent fractionation line between the chondrules and the solar value (Clayton et al., 1973; see also Scott et al., 2018, and references therein). (2) CAIs contain evidence for the former presence of ^{10}Be, which most likely originated from spallation by cosmic rays during the early phases of the sun's formation when energetic particles from magnetic reconnection flares irradiated materials at the inner edge of the protosolar accretion disk (McKeegan et al., 2000; Marhas et al., 2002; Chaussidon et al., 2006). This points towards CAIs originating near the infant Sun. (3) CAIs, where least affected by subsequent processes, are generally inferred to represent high-temperature condensates under conditions of low oxygen fugacity (Simon et al., 2005; Grossman et al., 2008b).

In contrast, however, there is an array of observations from isotopes of other elements (now including Sr, as set out here and in Charlier et al., 2017, through the availability of double-spike data) to suggest that CAIs have some affinity with the bulk carbonaceous chondrites, which most likely derived from external regions of the solar system (beyond the orbit of Jupiter: Kruijer et al., 2017). Because the CAIs studied so far are overwhelmingly found within carbonaceous chondrites, their formation close to the Sun requires that their transfer to the outer solar system was rapid enough to preserve high-temperature assemblages and a wide variation in textural types (Wood, 2004, for review). Such rapid transport is consistent with recent modelling results in which the effect of cloud collapse and angular momentum conservation during formation of the protoplanetary disk are accounted for (Yang & Ciesla 2012; Pignatale et al., 2018). It is also consistent with noble gas systematics in the, for example, Murchison meteorite (Kööp et al., 2018), where

some high-temperature CAI materials (e.g. hibonite-rich CAIs) show evidence for exposure as individual entities for periods of 3-100 Myr under conditions cold enough to preclude diffusive losses, before incorporation into the Murchison parent body.

Overall, outer solar system materials represented by many carbonaceous and some primitive achondrite meteorite types have resolvable differences in their bulk isotopic systematics for several elements when compared to the inner solar system materials that are representative of the terrestrial planets and differentiated asteroids (e.g. Warren, 2011). When shown in bivariate plots, these differences are reflected in two distinct clusters of data for the 'inner' and 'outer' materials, for example, in Ti and Cr (Warren, 2011), Ni (Render et al., 2018; Nanne et al., 2019) and Sr (Charlier et al., 2017) (see also Dauphas and Schauble, 2016, for an overview and other examples). This clustering of data is also preserved when the relevant bulk meteorite data are plotted versus $\Delta^{17}O$ (e.g. Dauphas and Schauble, 2016; Scott et al., 2018), the values of which are generally used to infer a high-temperature, near-sun source for the CAIs.

The Sr isotopic data we present here and those from other isotopic systems thus illustrate what one might call the 'CAI conundrum', that is, that CAIs originate in high-temperature, near-sun conditions, yet show several key isotopic features closely parallel with those of their host meteorites that came from sources in the outer solar system. Based on this similarity, specifically for Mo isotopic anomalies, Brennecka et al. (2018) suggested that fine-grained CAIs also were formed beyond the orbit of Jupiter. They argued that the early-forming Jupiter may have released sufficient heat to generate conditions suitable for high-temperature condensation in its vicinity (although see also MacPherson, 2019). The CAIs that we have analysed for Sr isotopes from Allende share the same 'outer' characteristics with the bulk Allende and other carbonaceous chondrite data presented by Charlier et al (2017) and are clearly distinct from the 'inner', terrestrial field. We have no simple explanation for this relationship. CAIs are enriched in refractory elements but mass-balance estimates show that they are not the sole carrier of Sr, Ti and other refractory elements in carbonaceous chondrites (Burkhardt et al., 2012). One

possibility is that carbonaceous chondrites inherited much of their refractory element isotopic signatures from a cryptic refractory dust (CRD) component (Dauphas and Pourmand, 2015; Barrat et al., 2016). This dust is in addition to the CAIs but is now unrecognizable due to its processing and mixing with carbonaceous chondrite matrix. An important observation bearing on this issue is that while CAIs and carbonaceous chondrites may share some genetic ties, there are clear distinctions between the two. To illustrate this point, we plot the ε^{50}Ti data from Davis et al. (2018) versus the internally normalised μ^{84}Sr values from this paper for the same CAI samples (Fig. 10). We also compare these data with the ε^{50}Ti values (Dauphas and Schauble, 2016, and references therein) from selected bulk meteorites representative of diverse parent bodies in the 'inner' and outer' solar system versus their corresponding μ^{84}Sr values from Charlier et al. (2017: see Table S3). The contrast in bulk meteorite compositions between 'inner' and 'outer' groupings is clear, but the CAI data show more extreme variations. The cluster of CAI data centred around ε^{50}Ti = +9 was remarked on by Davis et al. (2018, their figure 4) and the centre of this cluster is similar in its μ^{84}Sr value to those of the bulk carbonaceous chondrites (i.e., around 100 ppm, as seen in the three-isotope plot for Sr isotopes in Charlier et al., 2017). In the context of our hypothesis that the existence of a CRD component controls the isotope composition of bulk meteorites, this CRD must be characterized by isotope anomalies in Sr and Ti of smaller magnitude than those observed in CAIs (Fig 10). Similar CRD components might not be restricted to carbonaceous meteorites as shown by recent Ti isotope data obtained in CAIs and Na-Al-rich chondrules in ordinary and CO chondrites (Ebert et al., 2018).

Nonetheless, even if it is considered that the CAI materials in the Allende meteorite, transported outwards from their inferred near-solar source, were essentially Rb-free and that all the Rb-Sr relationships documented here reflect processes in the 'outer' solar system, this cannot explain why other diverse isotope systems show parallel 'inner'-'outer' dichotomies. In particular, it is not clear why μ^{84}Sr values should be offset if CAIs were derived from an 'inner' source that subsequently formed the reservoir for the terrestrial planets and differentiated meteorites. The trends seen on bivariate plots of various isotopes, for example, ε^{50}Ti, ε^{54}Cr, ε^{62}Ni and μ^{84}Sr (e.g.

Fig. 10), including when plotted against $\Delta^{17}O$ (e.g. Scott et al., 2018) show that materials with the 'outer' characteristics define trends that do not point towards the field of the 'inner' materials in many cases, suggesting that the 'outer' trends involve mixing relationships between two (or more) reservoirs, the characteristics of which are yet to be established.

5. Conclusions

Our new double-spike and internally-normalised Sr-isotopic data, when coupled with constraints from Rb-Sr relationships and Eu and Sm abundance patterns bring new perspectives to the complex genesis of Allende CAIs. The CAIs all have elevated nucleosynthetic $\mu^{84}Sr$ values with an average of +110 ppm, but with a range from +54 ppm to +287 ppm - far exceeding analytical precision. The average $\mu^{84}Sr$ is identical within error to that yielded by bulk carbonaceous chondrites, including Allende, that are most likely derived from the outer solar system. Part of the $\mu^{84}Sr$ diversity in CAIs may arise from the sporadic presence of high-$\mu^{84}Sr$ components ('nuggets'). These components pull the data towards positive values in Allende, whereas published data from leaching experiments of the CI chondrite Ivuna trend towards strongly negative values in the more chemically-resistant components.

An Rb-Sr errorchron from all our CAI data yields an errorchron of 4507 ± 23 Ma and an intercept of $^{87}Sr/^{86}Sr = 0.69886 \pm 20$, the latter figure being within error of previously published 'ALL' values. In elemental terms, both our coarse- and fine-grained CAIs show a close linear co-variation between Sr and Eu (normalised to CI chondrite values then ratioed to Th), despite their nominal contrasts in condensation temperatures. This may indicate that Eu behaved as $Eu^{2}+$, closely accompanying $Sr^{2}+$ in condensing minerals.

The CAI double-spike data yield an MDFL that is offset with respect to the equilibrium MDFL for differentiated meteorite and terrestrial samples in three-isotope space ($\delta^{88/86}Sr$ versus $\delta^{84/86}Sr$), and is within error the same as that derived from bulk samples of primitive meteorites (including Allende), but with greater scatter. Our data alone cannot distinguish between *p*-process anomalies in ^{84}Sr

versus *r-*, and weak and main *s*-process variability in ^{88}Sr. However, consideration of published ^{84}Sr CAI data (especially from the FUN inclusions) suggests that the anomaly likely resides in ^{84}Sr as initial $^{87}Sr/^{86}Sr$ values remain close to the canonical value for 'ALL' despite wide variations in $\mu^{84}Sr$ values. In turn, values of $\mu^{84}Sr$ for individual CAIs analysed here do not correlate with the degree of mass-dependent fractionation represented by the $\delta^{88/86}Sr$ value. Our CAIs that are depleted in Sr due to its greater volatility than Th or Sm show more variable $\delta^{88/86}Sr$ isotopic compositions, reflecting kinetic effects associated with partial condensation/ evaporation of Sr.

The picture given by the Sr isotopic variations presented here is that the CAIs analyzed share Sr-isotopic features in common with materials from other primitive and carbonaceous meteorites (i.e., derived from the outer solar system). The Sr isotopic data we present here and those published from other isotopic systems yield a conundrum, that is, CAIs are conventionally inferred to have formed in near-sun conditions, yet show several key isotopic features closely parallel with sources in the outer solar system. More work is needed to understand why CAIs and carbonaceous chondrites share these similarities, one possibility being that much of the inventory of refractory elements in carbonaceous chondrites was transported from the inner part of the solar system (the CAI-forming region) but that this dust component is largely unrecognizable today due to subsequent processing and mixing with carbonaceous chondrite matrix.

Acknowledgements

We thank Greg Brennecka, Glenn MacPherson and two anonymous reviewers for their thorough and incisive reviews which helped clarify our presentation and thinking. We also thank Qing-zhu Yin for his comments and Jeffrey Catalano for final editorial handling. This work was supported by a Crosby Postdoctoral Fellowships (MIT) and NSF grant (EAR1824002) to FT, and NASA grants NNX17AE86G (LARS), NNX17AE87G (Emerging Worlds), and 80NSSC17K0744 (Habitable Worlds) to ND.

References

Andreasen, R. and Sharma, M. (2007) Mixing and homogenization in the early solar system: clues from Sr, Ba, Nd, and Sm isotopes in meteorites. *Astrophys. J.* **665**, 874-883.

Amelin, Y., Kaltenbach, A., Iizuka, T., Stirling, C. H., Ireland, T. R., Petaev, M. and Jacobsen, S. B. (2010) U-Pb chronology of the Solar System's oldest solids with variable $^{238}U/^{235}U$. *Earth Planet. Sci. Lett.* **300**, 343-350.

Amelin, Y., Williams, C.D. and Wadhwa, M. (2015). U-Th-Pb and Rb-Sr systematics of Allende FUN CAI CMS-1. *Proc. 46th Lunar and Planetary Science Conference*, 2355.

Arlandini, C., Käppeler, F., Wisshak, K., Gallino, R., Lugaro, M., Busso, M. and Straniero, O. (1999) Neutron capture in low-mass asymptotic giant branch stars: cross sections and abundance signatures. *Astrophys. J.* **525**, 886-900.

Barrat, J.A., Dauphas, N., Gillet, P., Bollinger, C., Etoubleau, J., Bischoff, A. and Yamaguchi, A. (2016). Evidence from Tm anomalies for non-CI refractory lithophile element proportions in terrestrial planets and achondrites. *Geochim. Cosmochim. Acta* **176,** 1-17.

Beckett, J.R. and Grossman, L. (1986) Oxygen fugacities in the solar nebula during crystallization of fassaite in Allende inclusions. *Proc. Lunar Planet. Sci*. **XVII**, 36-37.

Bisterzo, S., Travaglio, C., Gallino, R., Wiescher, M. and Kappeler, F. (2014) Galactic chemical evolution and solar *s*-process abundances: Dependence on the ^{13}C-pocket structure. *Astrophys. J.* **787**, 10-24.

Boehnke P., Steele R. C. J., Tissot F. L. H. and Davis A. M. (2018) Calculating isotope anomalies: a Bayesian approach. *28th Annual V.M. Goldschmidt Conference,* August 12-17, 2018, Boston, USA, 220.

Boynton, W. V., 1975. Fractionation in the solar nebula: condensation of yttrium and the rare earth elements. *Geochim. Cosmochim. Acta* **39**, 569-584.

Boynton, W. V., 1989. Cosmochemistry of the rare-earth elements: condensation and evaporation processes. In *Geochemistry and mineralogy of rare earth elements* (eds. B. Lipin and G. A. McKay). *Rev. Mineral. Geochem.* **21**, 1-24.

Brearley, A. J., 2014. Nebular versus parent-body processing. In *Meteorites and cosmochemical processes* (ed. A. M. Davis), *Treatise on Geochemistry* (2nd Edition). Elsevier, Amsterdam, pp. 309-334.

Brennecka, G. A., Borg, L. E. and Wadhwa, M. (2013) Evidence for supernova injection into the solar nebula and decoupling of *r*-process nucleosynthesis. *Proc. Nat. Acad. Sci. USA* **110**, 17241-17246.

Brennecka, G. A., Burkhardt, C., Kruijer, T. S. and Kleine, T. (2017) Towards understanding the source of nucleosynthetic anomalies in refractory inclusions. *Proc. 48th Lunar and Planetary Science Conference*, 1619.

Brennecka, G. A., Burkhardt, C., Nimmo, F., Kruijer, T. S. and Kleine, T. (2018) Molybdenum isotopic evidence for a distal formation of refractory inclusions. *Proc. 49th Lunar and Planetary Science Conference*, 2429.

Burkhardt, C., Kleine, T., Oberli, F., Pack, A., Bourdon, B. and Wieler, R. (2011) Molybdenum isotope anomalies in meteorites: constraints on solar nebula evolution and origin of the Earth. *Earth Planet. Sci. Lett.* **312**, 390-400.

Burkhardt, C., Kleine, T., Dauphas, N. and Wieler, R. (2012) Origin of isotopic heterogeneity in the solar nebula by thermal processing and mixing of nebular dust. *Earth Planet. Sci. Lett.* **357-358**, 298-307.

Charlier, B. L. A., Nowell, G. M., Parkinson, I. J., Kelley, S. P., Pearson, D. G. and Burton, K. W. (2012) High temperature strontium stable isotope behaviour in the early solar system and planetary bodies. *Earth Planet. Sci. Lett.* **329-330**, 31–40.

Charlier, B. L. A., Parkinson, I. J., Burton, K. W., Grady, M. M., Wilson, C. J. N. and Smith, E. G. C. (2017) Stable strontium isotopic heterogeneity in the solar system from double-spike data. *Geochem. Perspec. Lett.* **4**, 35-40.

Chaussidon, M., Robert, F. and McKeegan, K. D. (2006) Li and B isotopic variations in an Allende CAI: evidence for the in situ decay of short-lived ^{10}Be and for the possible presence of the short-lived nuclide ^{7}Be in the early solar system. *Geochim. Cosmochim. Acta* **70**, 224-245.

Clayton, D. D. (1977) Cosmoradiogenic ghosts and the origin of Ca-Al-rich inclusions. *Earth Planet. Sci. Lett.* **35**, 398-410.

Clayton, R. N., Grossman, L. and Mayeda, T. K. (1973) A component of primitive nuclear composition in carbonaceous meteorites. *Science* **182**, 485-498.

Connelly, J. N., Bizzarro, M., Krot, A. N., Nordlund, Å, Wielandt, D. and Ivanova, M. A. (2012) The absolute chronology and thermal processing of solids in the solar protoplanetary disk. *Science* **338**, 651-655.

Dauphas, N. and Rouxel, O. (2006) Mass spectrometry and natural variations of iron isotopes. *Mass Spectrom. Rev.* **25**, 515-550.

Dauphas, N. and Schauble, E. A. (2016) Mass fractionation laws, mass-independent effects, and isotopic anomalies. *Ann. Rev. Earth Planet. Sci.* **44**, 709-783.

Dauphas, N., Poitrasson, F., Burkhardt, C., Kobayashi, H. and Kurosawa, K. (2015) Planetary and meteoritic Mg/Si and δ^{30}Si variations inherited from solar nebula chemistry. *Earth Planet. Sci. Lett.* **427**, 236-248.

Dauphas, N. and Pourmand, A. (2015) Thulium anomalies and rare earth element patterns in meteorites and Earth: nebular fractionation and the nugget effect. *Geochim. Cosmochim. Acta* **163,** 234-261.

Davis, A. M. and Grossman, L. (1979) Condensation and fractionation of rare earths in the solar nebula. *Geochim. Cosmochim. Acta* **43**, 1611-1632.

Davis, A. M., Richter, F. M., Mendybaev, R. A., Janney, P. E., Wadhwa, M. and McKeegan, K. D. (2015) Isotopic mass fractionation laws for magnesium and their effects on ^{26}Al-^{26}Mg systematics in solar system materials. *Geochim. Cosmochim. Acta* **158**, 245-261.

Davis, A. M., Zhang, J., Greber, N. D., Hu, J., Tissot, F. L. H. and Dauphas, N. (2018) Titanium isotopes and rare earth patterns in CAIs: evidence for thermal processing and gas-dust decoupling in the protoplanetary disk. *Geochim. Cosmochim. Acta* 221, 275-295.

Desch, S. J., Kalyaan, A. and Alexander, C. M. O'D. (2018) The effect of Jupiter's formation on the distribution of refractory elements and inclusions in meteorites. *Astrophys. J. Suppl. Ser.* **238**, article 11.

Dodson, M. H. (1963) A theoretical study of the use of internal standards for precise isotopic analysis by the surface ionization technique: Part I - General first-order algebraic solutions. *J. Sci. Instrum.* **40**, 289-295.

Ebert, S., Render, J., Brennecka, G. A., Burkhardt, C., Bischoff, A., Gerber, S. and Kleine, T. (2018) Ti isotopic evidence for a non-CAI refractory component in the inner solar system. *Earth Planet. Sci. Lett.* **498**, 257-265.

Gray, C. M., Papanastassiou, D. A. and Wasserburg, G. J. (1973) The identification of early condensates from the solar nebula. *Icarus* **20**, 213-239.

Grossman, L. (1972) Condensation in the primitive solar nebula. *Geochim. Cosmochim. Acta* **36**, 597-619.

Grossman, L. (1975) Petrography and mineral chemistry of Ca-rich inclusions in the Allende meteorite. *Geochim. Cosmochim. Acta* **39**, 433-454.

Grossman, L., Ganapathay, R. and Davis, A. M. (1977) Trace elements in the Allende meteorite—III. Coarse-grained inclusions revisited. *Geochim. Cosmochim. Acta* **41**, 1647-1664.

Grossman, L., Simon, S. B., Rai, V. K., Thiemens, M. H., Hutcheon, I. D., Williams, R. W., Galy, A., Ding, T., Fedkin, A. V., Clayton, R. N. and Mayeda, T.K. (2008a) Primordial compositions of refractory inclusions. *Geochim. Cosmochim. Acta* **72**, 3001-3021.

Grossman, L., Beckett, J. R., Fedkin, A.V., Simon, S. B. and Ciesla, F. J. (2008b) Redox conditions in the solar nebula: observational, experimental, and theoretical constraints. *Rev. Mineral. Geochem.* **68**, 93-140.

Halliday, A. N. and Porcelli, D. (2001) In search of lost planets – the paleocosmochemistry of the inner solar system. *Earth Planet. Sci. Lett.* **192,** 545-559.

Hans, U., Kleine, T. and Bourdon, B. (2013) Rb–Sr chronology of volatile depletion in differentiated protoplanets: BABI, ADOR and ALL revisited. *Earth Planet. Sci. Lett.* **374**, 204–214.

Hashimoto, A. and Grossman, L. (1987) Alteration of Al-rich inclusions inside amoeboid olivine aggregates in the Allende meteorite. *Geochim. Cosmochim. Acta* **51**, 1685-1704.

Huss, G. R., Rubin, A. E. and Grossman, J. N. (2006) Thermal metamorphism in chondrites. In *Meteorites and the early solar system II* (eds. D. Lauretta, L. A. Leshin and H. Y. McSween,). Tucson, Arizona, University of Arizona Press, pp. 567–586.

Jacobsen B., Yin Q. -Z., Moynier F., Amelin Y., Krot A. N., Nagashima K., Hutcheon I. D. and Palme, H. (2008) ^{26}Al-^{26}Mg and ^{207}Pb-^{206}Pb systematics of Allende CAIs: Canonical solar initial ^{26}Al/^{27}Al ratio reinstated. *Earth. Planet. Sci. Lett.* **272**, 353–364.

Kappeler, F., Beer, H. and Wisshak, K. (1989) *s*-Process nucleosynthesis-nuclear physics and the classical model. *Rep. Progr. Phys.* **52**, 945-1013.

Keil, K. (2012) Angrites, a small but diverse suite of ancient, silica-undersaturated volcanic-plutonic mafic meteorites, and the history of their parent asteroid. *Chem. Erde* **72,** 191-218.

Kimura M. and Ikeda Y. (1995) Anhydrous alteration of Allende chondrules in the solar nebula II: Alkali-Ca exchange reactions and formation of nepheline, sodalite, and Ca-rich phases in chondrules. *Proc. NIPR Symp. Antarctic Meteorites* **8**, 123–138.

Kööp, L., Heck, P. R., Busemann, H., Davis, A. M., Greer, J., Maden, C., Meier, M. M. M. and Wieler, R. (2018) High early solar activity inferred from helium and neon excesses in the oldest meteorite inclusions. *Nature Astron*. **2**, 709-713.

Kornacki, A. S. and Fegley Jr, B. (1986) The abundance and relative volatility of refractory trace elements in Ca, Al-rich inclusions: implications for chemical and physical processes in the solar nebula. *Earth Planet. Sci. Lett.* **79**, 217-234.

Krot, A. N., Scott, E. R. D. and Zolensky, M.E. (1995) Mineralogical and chemical modification of components in CV3 chondrites: nebular or asteroidal processing? *Meteoritics* **30**, 748-775.

Krot, A. N., MacPherson, G. J., Ulyanov, A. and Paetev, I. (2004) Fine-grained, spinel-rich inclusions from the reduced CV chondrites Efremovka and Leoville: I. Mineralogy, petrology, and bulk chemistry. *Meteorit. Planet. Sci.* **39**, 1517-1553.

Kruijer, T. S., Burkhardt, C., Budde, G. and Kleine, T. (2018) Age of Jupiter inferred from the distinct genetics and formation times of meteorites. *Proc. Nat. Acad. Sci. USA* **114**, 6712-6716.

Lodders, K. (2003) Solar system abundances and condensation temperatures of the elements. *Astrophys. J.* **591**, 1220-1247.

Ludwig, K. R. (2002) *Isoplot/Ex Version 2.49: a geochronological toolkit for Microsoft Excel*. Berkeley, CA: Berkeley Chronology Center.

Lugaro, M., Herwig, F., Lattanzio, J. C., Gallino, R. and Straniero, O. (2003) *s*-Process nucleosynthesis in asymptotic giant branch stars: A test for stellar evolution. *Astrophys. J.* **586**, 1305-1319.

MacPherson, G. J. (2014) Calcium-aluminum-rich inclusions in chondritic meteorites. In *Meteorites and cosmochemical processes* (ed. A. M. Davis), *Treatise on Geochemistry* (2nd Edition). Elsevier, Amsterdam, pp. 139-179.

MacPherson, G. J. (2019) CAIs did not form in the outer solar system. *Proc. 50th Lunar and Planetary Science Conference*, 3005.

MacPherson, G. J. and Davis, A. M. (1993) A petrologic and ion microprobe study of a Vigarano Type B refractory inclusion: Evolution by multiple stages of alteration and melting. *Geochim. Cosmochim. Acta* **57**, 231-243.

MacPherson, G. J., Wark, D. A. and Armstrong, J. T. (1988) Primitive material surviving in chondrites: refractory inclusions. In *Meteorites and the early solar system* (eds. J. F. Kerridge and M. S. Matthews). Tucson, University of Arizona Press, pp. 746-807.

MacPherson G. J., Kita, N. T., Ushikubo, T., Bullock, E. S. and Davis, A. M. (2012) Well-resolved variations in the formation ages for Ca-Al-rich inclusions in the early solar system. *Earth Planet. Sci. Lett.* **331-332**, 43-54.

MacPherson, G. J., Nagashima, K., Krot, A. N., Doyle, P. M. and Ivanova, M. A. (2015) ^{53}Mn-^{53}Cr systematics of Ca-Fe silicates in CV3 chondrites. *Proc. 46th Lunar and Planetary Science Conference*, 2760.

MacPherson, G. J., Defouilloy, C. and Kita, N. T. (2018) High-precision Al–Mg isotopic systematics in *USNM 3898* – The benchmark "ALL" for initial ^{87}Sr/^{86}Sr in the earliest Solar System. *Earth Planet. Sci. Lett.* **491**, 238-243.

Maréchal, C. N., Télouk, P. and Albarède, F. (1999) Precise analysis of copper and zinc isotopic compositions by plasma-source mass spectrometry. *Chem. Geol.* **156**, 251-273.

Marhas, K. K., Goswami, J. N. and Davis, A. M. (2002) Short-lived nuclides in hibonite grains from Murchison: evidence for solar system evolution. *Science* **298**, 2182-2185.

Marks, N. E., Borg, L. E., Hutcheon, I. D, Jacobsen, B. and Clayton, R. N. (2014) Samarium-neodymium chronology and rubidium-strontium systematics of an Allende calcium-aluminum-rich inclusion with implications for ^{146}Sm half-life. *Earth Planet. Sci. Lett.* **405**, 15-24.

McKeegan, K. D., Chaussidon, M. and Robert, F. (2000) Incorporation of short-lived ^{10}Be in a calcium-aluminum-rich inclusion from the Allende meteorite. *Science* **289**, 1134-1137.

Meeker, G. P., Wasserburg, G. J. and Armstrong, J. T. (1983) Replacement textures in CAI and implications regarding planetary metamorphism. *Geochim. Cosmochim. Acta* **47**, 707-721.

Moynier, F., Agrainer, A., Hezel, D. C. and Bouvier, A. (2010) Sr stable isotope composition of Earth, the Moon, Mars, Vesta and meteorites. *Earth Planet. Sci. Lett.* **300**, 359–366.

Moynier, F., Day, J. M. D., Okui, W., Yokoyama, T., Bouvier, A., Walker, R. J. and Podosek, F. A. (2012) Planetary-scale strontium isotopic heterogeneity and the age of volatile depletion of early solar system materials. *Astrophys. J.* **758**, 45.

Myojo, K., Yokoyama, T., Okabayashi, S., Wakaki, S., Sugiura, N. and Iwamori, H. (2018) The origin and evolution of nucleosynthetic Sr isotope variability in calcium and aluminium-rich refractory inclusions. *Astrophys. J.* **853**, 48.

Nanne, J. A. M., Nimmo, F., Cuzzi, J. N. and Kleine, T. (2019) Origin of the non-carbonaceous–carbonaceous meteorite dichotomy. *Earth Planet. Sci. Lett.* **511**, 44-54.

Neymark, L. A., Premo, W. R., Mel'nikov, N. N. and Emsbo, P. (2014) Precise determination of δ^{88}Sr in rocks, minerals and waters by double-spike TIMS: a powerful tool in the study of geological, hydrological and biological processes. *J. Anal. Atom. Spectrom.* **29**, 65-75.

Niederer, F. R. and Papanastassiou, D. A. (1984) Ca isotopes in refractory inclusions. *Geochim. Cosmochim. Acta* **48**, 1279-1293.

Nyqyist, L. E., Shih, C.-Y. and Takeda, H. (2004) Chronology of eucrite petrogenesis from Sm-Nd and Rb-Sr systematics. *Proc. 28th Symp Antarctic Meteorites. Antarctic Meteorite Research* **18**, 66-67. National Institute of Polar Research, Tokyo, Japan.

Palme, H., Lodders, L. and Jones, A. (2014) Solar system abundances of the elements. In *Meteorites and cosmochemical processes* (ed. A. M. Davis), *Treatise on Geochemistry* (2nd Edition). Elsevier, Amsterdam, pp. 15-36.

Papanastassiou, D. A. (2015) Initial ^{87}Sr/^{86}Sr chronology; a journey through 4.5 decades. *Proc. 46th Lunar and Planetary Science Conference*, 2243.

Papanastassiou, D. A. and Chen, J. H. (2016) Initial $^{87}Sr/^{86}Sr$ chronology in the solar system. *Proc. 47th Lunar and Planetary Science Conference*, 2650.

Papanastassiou, D. A. and Wasserburg, G. J., (1969) Initial strontium isotopic abundances and the resolution of small time differences in the formation of planetary bodies. *Earth Planet. Sci. Lett.* **5**, 361–376.

Papanastassiou, D. A. and Wasserburg, G. J. (1978) Strontium isotopic anomalies in the Allende meteorite. *Geophys. Res Lett.* **5**, 595–598.

Patchett, P. J. (1980a) Sr isotopic fractionation in Ca–Al inclusions from the Allende meteorite. *Nature* **283**, 438–441.

Patchett, P. J. (1980b) Sr isotopic fractionation in Allende chondrules: a reflection of solar nebular processes. *Earth Planet. Sci. Lett.* **50**, 181–188.

Paton, C., Schiller, M. and Bizzarro, M. (2013) Identification of an ^{84}Sr-depleted carrier in primitive meteorites and implications for thermal processing in the solar protoplanetary disk. *Astrophys. J. Lett*. **763**, L40.

Pignatale, F. C., Charnoz, S., Chaussidon, M. and Jacquet, E. (2018) Making the planetary material diversity during the early assembling of the solar system. *Astrophys. J. Lett.* **867,** L23.

Podosek, F. A., Zinner, E. K., MacPherson, G. J., Lundberg, L. L., Brannon, J. C. and Fahey, A. J. (1991) Correlated study of initial $^{87}Sr/^{86}Sr$ and Al-Mg isotopic systematics and petrologic properties in a suite of refractory inclusions from Allende meteorite. *Geochim. Cosmochim. Acta* **55**, 1083-1110.

Pravdivtseva, O. V., Krot, A. N., Hohenberg, C. M., Meshik, A. P., Weisberg, M. K. and Keil, K. (2003) The I-Xe record of alteration in the Allende CV chondrite. *Geochim. Cosmochim. Acta* **64**, 5011-5026.

Rauscher, T., Heger, A., Hoffman, R. D. and Woosley, S. E. (2002) Nucleosynthesis in massive stars with improved nuclear and stellar physics. *Astrophys. J.* **576**, 323-348.

Render, J., Brennecka, G. A., Wang, S. -J., Wasylenki, L. E. and Kleine, T. (2018) A distinct nucleosynthetic heritage for early solar system solids recorded by Ni isotope signatures. *Astrophys. J.* **862,** 26.

Richter, F. M. (2004) Timescales determining the degree of kinetic isotope fractionation by evaporation and condensation. *Geochim. Cosmochim. Acta* **68**, 4971-4992.

Richter, F. M., Janney, P. E., Mendybaev, R. A., Davis, A. M. and Wadhwa, M. (2007) Elemental and isotopic fractionation of Type B CAI-like liquids by evaporation. *Geochim. Cosmochim. Acta* **71**, 5544-5564.

Rosman, K. J. R. and Taylor, P. D. P. (1998) Isotopic composition of the elements 1997. *Pure Appl. Chem*. **70**, 217-235.

Rotenberg, E., Davis, D. W., Amelin, Y., Ghosh, S. and Bergquist, B. A. (2012) Determination of the decay-constant of ^{87}Rb by laboratory accumulation of ^{87}Sr. *Geochim. Cosmochim. Acta* **85**, 41-57.

Rudge, J. F., Reynolds, B. C. and Bourdon, B. (2009) The double spike toolbox. *Chem. Geol.* **265**, 420-431.

Russell S. S. and MacPherson G. J. (1997) Alteration of calcium-aluminum-rich inclusions: times and places. In *Workshop on parent-body and nebular modification of chondritic materials* (eds. M. E. Zolensky, A. N. Krot and E. R. D. Scott). *LPI Technical Report* **97–02**, pp. 54-55. Lunar and Planetary Institute, Houston, Texas, USA.

Scott, E. R. D. and Krot, A. N. (2014) Chondrites and their components. In *Meteorites and cosmochemical processes* (ed. A. M. Davis), *Treatise on Geochemistry* (2nd Edition). Elsevier, Amsterdam, pp. 65-137.

Scott, E. R. D., Krot, A. N. and Sanders, I. S. (2018) Isotopic dichotomy among meteorites and its bearing on the protoplanetary disk. *Astrophys. J.* **854**, 164.

Shahar, A. and Young, E. D. (2007) Astrophysics of CAI formation as revealed by silicon isotope LA-MC-ICPMS of an igneous CAI. *Earth Planet. Sci. Lett.* **257**, 497-510.

Shollenberger, Q. R., Borg, L. E., Render, J., Ebert, S., Bischoff, A., Russell, S. S. and Brennecka, G. A. (2018a) Isotopic coherence of refractory inclusions from CV and CK meteorites: Evidence from multiple isotope systems. *Geochim. Cosmochim. Acta* **228**, 62-80.

Shollenberger, Q. R., Render, J. and Brennecka, G. A. (2018b) Er, Yb, and Hf isotopic compositions of refractory inclusions: an integrated isotopic fingerprint of the Solar System's earliest reservoir. *Earth Planet. Sci. Lett.* **495**, 12-23.

Simon, J. I. and DePaolo, D. J. (2010) Stable calcium isotopic composition of meteorites and rocky planets. *Earth Planet. Sci. Lett.* **289**, 457-466.

Simon, J. I., Young, E. D., Russell, S. S., Tonui, E. K., Dyl, K. A. and Manning, C. E. (2005) A short timescale for changing oxygen fugacity in the solar nebula revealed by high-resolution ^{26}Al-^{26}Mg dating of CAI rims. *Earth Planet. Sci. Lett.* **238**, 272-283.

Simon, J. I., Jordan, M. K., Tappa, M. J., Schauble, E. A., Kohl, I. E. and Young, E. D. (2017) Calcium and titanium isotope fractionation in refractory inclusions: tracers of condensation and inheritance in the early solar protoplanetary disk. *Earth Planet. Sci. Lett.* **472**, 277-288.

Tang, H. and Dauphas, N. (2012) Abundance, distribution, and origin of ^{60}Fe in the solar protoplanetary disk. *Earth Planet. Sci. Lett.* **359-360**, 248-263.

Tang, H., Liu, M.-C., McKeegan, K. D., Tissot, F. L. H. and Dauphas, N. (2017) *In situ* isotopic studies of the U-depleted Allende CAI *Curious Marie*: pre-accretionary alteration and the co-existence of ^{26}Al and ^{36}Cl in the early solar nebula. *Geochim. Cosmochim. Acta* **207**, 1-18.

Tissot F. L. H., Dauphas N. and Grossman L. (2016) Origin of uranium isotope variations in early solar nebula condensates. *Sci. Adv.* **2**, e1501400.

Tissot, F. L. H., Dauphas, N. and Grove, T. L. (2017) Distinct ^{238}U/^{235}U ratios and REE patterns in plutonic and volcanic angrites: geochronologic implications and evidence for U isotope fractionation during magmatic processes. *Geochim. Cosmochim. Acta* **213**, 593-617.

Tissot, F. L. H., Burkhardt, C., Budde, G. and Kleine, T. (2019) Multi-elemental and isotopic characterization of coarse-grained Allende CAIs. *Proc. 50th Lunar and Planetary Science Conference*, 3136.

Travaglio, C., Gallino, R., Arnone, E. Cowan, J., Jordan, F. and Sneden, C. (2004) Galactic evolution of Sr, Y and Zr: a multiplicity of nucleosynthetic processes. *Astrophys. J.* **601**, 864-884.

Trinquier, A., Elliot, T., Ulfbeck, D., Coath, C., Krot, A. N. and Bizzarro, M. (2009) Origin of nucleosynthetic isotope heterogeneity in the solar proplanetary disk. *Science* **324**, 374-376.

Wänke, H., Baddenhausen, H., Palme, H. and Spettel, B. (1974) On the chemistry of the Allende inclusions and their origin as high temperature condensates. *Earth Planet. Sci. Lett.* **23**, 1-7.

Warren, P. H. (2011) Stable-isotopic anomalies and the accretionary assemblage of the Earth and Mars: a subordinate role for carbonaceous chondrites. *Earth Planet. Sci. Lett.* **311**, 93-100.

Wasserburg, G.J., Wimpenny, J. and Yin, Q.Z. (2012) Mg isotopic heterogeneity, Al-Mg isochrons, and canonical $^{26}Al/^{27}Al$ in the early solar system. *Meteor. Planet. Sci.* **47**, 1980-1997.

Wood, J. A. (2004) Formation of chondritic refractory inclusions: the astrophysical setting. *Geochim. Cosmochim. Acta* **68**, 4007-4021.

Yang, L. and Ciesla, F. J. (2012) The effects of disk building on the distributions of refractory materials in the solar nebula. *Met. Planet. Sci.* **47**, 99-119.

Yokoyama, T., Fukami, Y., Okui, W., Ito, N. and Yamazaki, H. (2015) Nucleosynthetic strontium isotope anomalies in carbonaceous chondrites. *Earth Planet. Sci. Lett.* **416**, 46-55.

Young, E. D., Galy, A. and Nagahara, H. (2002) Kinetic and equilibrium mass-dependent isotope fractionation laws in nature and their geochemical and cosmochemical significance. *Geochim. Cosmochim. Acta* **66**, 1095–1104.

Young, E. D., Manning, C. E., Schauble, E. A., Shahar, A., Macris, C. A., Lazar, C. and Jordan, M. (2015) High-temperature equilibrium isotope fractionation of non-traditional stable isotopes: Experiments, theory, and applications. *Chem. Geol.* **395**, 176-195.

Yurimoto, T., Krot, A. N., Choi, B. -G., Aleon, J., Kunihiro, T. and Brearley, A. J. (2008) Oxygen isotopes of chondritic components. *Rev. Mineral. Geochem.* **68,** 141-186.

Figure captions

Fig. 1. Plot of $\mu^{84}Sr$ for the data in this paper along with published data from other Allende CAIs (Moynier et al., 2012; Brennecka et al., 2013; Hans et al., 2013; Paton et al., 2013; Myojo et al., 2018). Note that for all these papers except Myojo et al. (2018) the textural classes of the CAIs (coarse- versus fine-grained) analysed can only be partially reconciled with earlier papers (Burkhardt et al., 2011; Brennecka et al., 2017). Myojo et al. (2018) presented twelve data points from 3 inclusions of types fluffy-type A: FTA); B; and fine-grained, spinel-rich (FS). The grey shaded bar represents the external reproducibility of 14 ppm 2 s.d. obtained in this study for the internally normalised $^{84}Sr/^{86}Sr$. The bottom panel shows the relative probability distribution curve and histogram for all Allende CAI $\mu^{84}Sr$ data. Red points denote coarse-grained CAIs, blue points denote fine-grained CAIs.

Fig. 2. $^{87}Rb/^{86}Sr$ versus $^{87}Sr/^{86}Sr$ errorchron plot for all CAI analyses. The best fit line was generated using a Type 3 fit to all the data using Isoplot (Ludwig, 2002). Results of individual regression to the fine- and coarse-grained CAIs are also given on the plot. Inset shows the age corrected (to 4507 Ma) $^{87}Sr/^{86}Sr$ values in ppm of individual CAI measurements and their displacement from the best fit line. Error bars smaller than symbol size in main panel, propagated uncertainty after age correction shown in inset panel.

Fig. 3. Plot of $\delta^{88/86}Sr$ vs $\delta^{84/86}Sr$ showing the data for the CAI samples in this study. Equilibrium MDFL denotes the equilibrium mass-dependent fractionation line (solid line) which passes through the origin (the assumed composition of NBS987) with a slope of -0.978 (Young et al., 2002). A best fit line (dot-dash line) to the angrite feldspar data from Charlier et al. (2017) is plotted as an example of the coherence of differentiated planetary materials to the equilibrium MDFL. A best fit line to all the CAI data presented here is offset from the equilibrium MDFL by +0.144 in $\delta^{84/86}Sr$. Uncertainties for all data points are smaller than the symbol size.

Fig. 4. Plot of $\mu^{84}Sr$ vs. $\delta^{88/86}Sr$ to show the lack of systematic variations between values of the nucleosynthetic anomaly ($\mu^{84}Sr$) and degree of mass-dependent fractionation ($\delta^{88/86}Sr$) for each CAI. Data are corrected using the exponential law, and coloured lines denote deviation in $\mu^{84}Sr$ if the power law and Rayleigh laws are used for fractionation correction (see text for details). Uncertainties in $\delta^{88/86}Sr$ values are smaller than symbol size.

Fig. 5 Plot of $\mu^{84}Sr$ vs. sample mass of CAIs digested by Tissot et al. (2016) and presented here. Grey shaded band represents the average $\mu^{84}Sr$, ± 2 s.e.

Fig. 6 Plots of (a) Rb/Th versus Sr/Th and (b) Eu/Th versus Sr/Th (chondrite normalised: data values from Table1; normalising values from Palme et al., 2014) for all the CAIs analysed here. Uncertainties for all data points are smaller than symbol size.

Fig. 7. Schematic plots (after Dauphas et al., 2015) to illustrate three possible scenarios to explain the stable Sr isotopic fractionation versus the elemental ratio of Sr (moderately volatile) to Sm (refractory) for the fine-grained CAIs investigated here. a. *Partial condensation followed by evaporation*. Initial condensates will be enriched in the light isotopes (negative $\delta^{88/86}Sr$) and have a low Sr/Sm ratios. Further condensation increases Sr/Sm and drives $\delta^{88/86}Sr$ towards heavier values (maximum of 0). At any stage, the partial condensates can be reheated and evaporated (two representative lines shown) to achieve positive $\delta^{88/86}Sr$ values. b. *Condensation only*, under different saturation conditions. Bottom curve represents $P/P_{sat} = 2$ (i.e., oversaturated resulting from undercooling where the system is 'rushed' into condensing); upper curve shows $P/P_{sat} = 1$ (equilibrium fractionation). The Δ_{eq} value of +2 ‰ is derived from that for Si isotopic fractionation in forsterite (Dauphas et al., 2015), assuming that there is similar fractionation for Si and Sr. c. *Mixing of variably condensed solid and gaseous components*. The black curve is the condensation curve from panels a and b, but note Sm/Sr is now plotted on the x-axis. The green dot is the composition of the first condensed solid which will be enriched in Sm, but have very little Sr; as in panels a and b, the associated $\delta^{88/86}Sr$ values will be light. The yellow dot represents the gas that remains after extensive condensation (low Sm/Sr,

heavy $\delta^{88/86}$Sr). Mixing of solids formed along the condensation path with the gas remaining after extensive condensation can generate the full range of data. The ranges in Sr/Sm ratios coupled with $\delta^{88/86}$Sr values imply that part at least of the stable isotope variations reflect processes other than simple condensation from a gaseous phase.

Fig. 8. Plots of (a) Rb versus Sr (values shown in ppm and chondrite normalised: data values from Table 1; normalizing values from Palme et al., 2014) for CAIs also analysed for stable strontium isotopes (this study and by Patchett, 1980a). (b) Double-spike $\delta^{88/86}$Sr values versus Sr abundance for our samples and those reported by Patchett (1980a). (c) μ^{84}Sr Values versus Sr abundance for our samples. We omit the data of Patchett (1980a) because the reported precision for ^{84}Sr in that paper spans the entire range of values presented here.

Fig. 9. (a): Plot of age-corrected ^{87}Sr/^{86}Sr values derived from the double-spike measurements versus $\delta^{88/86}$Sr values for all samples analysed. Uncertainties for all data points are smaller than symbol size. (b): Enlargement of the four coarse-grained CAI samples from panel (a) with a best fit line from these points alone(see text for details). (c) Plot of age-corrected ^{87}Sr/^{86}Sr values derived from the double-spike measurements versus $\delta^{84/86}$Sr values for the same four coarse-grained CAIs. Fully propagated uncertainties are shown as 2 s.d. error bars, including the uncertainties on the measured ^{87}Rb/^{86}Sr values used for age correction.

Fig. 10. Plot of ε^{50}Ti versus μ^{84}Sr in planetary materials and the CAIs studied in this paper. The ε^{50}Ti data are from Davis et al. (2018) for the CAIs, and Dauphas and Schauble (2016, and references therein) for the bulk planetary materials. The μ^{84}Sr data are from this paper for the CAIs (measured on the same samples as for the Ti data) and bulk planetary materials are the unpublished internally normalised data that are the counterpart to the data published in Charlier et al. (2017)(Table S3). See text for discussion.